



## Research article

# Investigating the thermo-physical properties of a new kind of graphitic carbon nitride included ternary hybrid nanofluids and the property correlations

Velu Nandakumar<sup>a,b</sup>, Chandravadhana Arumugam<sup>a,c</sup>,  
Padmanaban Radhakrishnan<sup>a</sup>, Vellaisamy A.L. Roy<sup>d</sup>, Gopalan Anantha-Iyengar<sup>e,f,\*</sup>,  
Dong-Eun Lee<sup>e,f,g</sup>, Venkatramanan Kannan<sup>a,\*\*</sup>

<sup>a</sup> Department of Physics, Sri Chandrasekharendra Saraswathi Viswa Mahavidyalaya, Kanchipuram, Tamil Nadu, 631 561, India

<sup>b</sup> Department of Physics, Maharani's Science College for Women (Autonomous), Mysuru, 570 005, India

<sup>c</sup> Department of Physics, S. A. Engineering College (Autonomous), Chennai, Tamil Nadu, 600 077, India

<sup>d</sup> School of Science and Technology, Hong Kong Metropolitan University, Ho Man Tin, Hong Kong

<sup>e</sup> Intelligent Construction Automation Center, Kyungpook National University, Daegu, 41566, Republic of Korea

<sup>f</sup> Kyungpook National University, Daegu, 41556, Republic of Korea

<sup>g</sup> School of Architecture, Civil, Environment and Energy, Kyungpook National University, 1370, Sangyeok-dong, Buk-gu, Daegu, 702701, Republic of Korea

## ARTICLE INFO

## Keywords:

Ternary hybrids  
Properties  
Nanofluids  
Stability  
Thermal conductivity

## ABSTRACT

In this work, a simple and facile approach was employed for the preparation of the ternary hybrids comprising of titanium dioxide, zinc oxide and graphitic nitride (designated as TZG-TH) with varying compositions of the components. In the context of complex and multi-stages involved for preparation of many of the THs in the literature, the present work uses the much simpler mythology for the preparation of TH. Nanofluids (NF) were formulated in ethylene glycol: water base fluid using TZG TH as the solid particles. Scanning electron microscope of TZG TH informs that the particles are agglomerated. High resolution transmission electron microscopy image of TZG-TH reveals the presence narrowly distributed spherical particles (having the sizes in the range 40 nm–100 nm) in sheet like structure. The core level X-ray photoelectron spectrum of carbon and nitrogen elements reveal the existence of sp<sup>2</sup>-bonded C in the C=N and pyridinic and graphitic nitrogen in TZG-TH. X-ray diffraction patterns of TZG TH show the existence of anatase and hexagonal phase wurtzite crystalline structure in TH. The thermo-physical properties were determined for the THNFs in order to elucidate the influence of compositions of the component and concentration of TZG-TH on the thermophysical properties. The TZG TH containing larger proportions of ZnO showed the maximum of 9.11 % and 12.1 % higher increase in viscosity than the binary and base fluid, respectively. The density of TZG THs varies from 1.079 to 1.095 cp, which is closer to the base fluid. The influence of TZG TH composition on refractive index and ultrasonic velocity indicates the existence of molecular level interactions between the nanoparticles in the TH and base fluid. The ~210 % thermal conductivity enhancement was witnessed for the TZG TH, which is significantly higher than that of ZnO mono NF (26.9%) and TiO<sub>2</sub> mono NF (33.0%). The influence of composition and concentration of TZG- TH on molecular interaction

\* Corresponding author. Intelligent Construction Automation Center, Kyungpook National University, Daegu 41566, Republic of Korea.

\*\* Corresponding author.

E-mail addresses: [algopal99@gmail.com](mailto:algopal99@gmail.com), [agopalan@knu.ac.kr](mailto:agopalan@knu.ac.kr) (G. Anantha-Iyengar), [kv@kanchiuniv.ac.in](mailto:kv@kanchiuniv.ac.in) (V. Kannan).

<https://doi.org/10.1016/j.heliyon.2024.e26163>

Received 2 July 2023; Received in revised form 22 November 2023; Accepted 8 February 2024

Available online 15 February 2024

2405-8440/Â© 2024 Published by Elsevier Ltd. This is an open access article under the CC BY-NC-ND license (<http://creativecommons.org/licenses/by-nc-nd/4.0/>).

parameters like adiabatic compressibility, intermolecular free length, free volume, internal pressure and specific acoustic impedance are reported. The TZG TH based NF showed adequate dispersion stability as inferred from dynamic light scattering and UV–visible spectroscopy results. The results on TZG TH included THNF are new to the literature and would be helpful in exploring multifunctional properties with heat transfer capabilities for applications.

## 1. Introduction

Ever since the proof of concept of nanofluids (NFs) has been demonstrated by Choi in 1995 [1] and associated enhancement of thermal conductivity (TC) of base fluid by dispersing micro/nano sized particles, the researches on NFs have flourished towards a significant progress. Subsequently, NFs were formulated with a variety of solid particles (metal, metal oxide, ceramics, carbon nanostructures etc.) and the results demonstrated higher heat transfer rates over base fluids [2,3]. It is important to infer from literature that the performances of NFs with the dispersion of single nanoparticles (mono NFs) are limited to provide the adequate heat transfer rates and other thermophysical properties as well stability [4]. To circumvent the limitations of mono NFs, hybrid nanofluids (HNFs) were developed by dispersing two or more nanoparticles (NPs) in the base fluid and the synergistic features of various NPs were derived [5,6]. HNFs prepared with various combination of metal and metal oxide NPs, exhibited higher TC and better stability over mono NFs [7,8]. However, the issues on long-term stability and ease of manufacturing process need to be resolved through the adequate use of combination of NPs [9]. This is a very much demanding and challenging task for the researchers.

Among the NFs, titanium dioxide (TiO<sub>2</sub>) NP based NFs received greater attraction due to their wide range of applicability, lower cost, and unique combination of properties like TC, photocatalytic activity and dielectric properties [10]. Taking the special advantages of TiO<sub>2</sub>, hybrid NFs have been formulated with other metal/metal oxide/carbon nanomaterials. A significant improvement in the TC of TiO<sub>2</sub> NFs was noticed with a deleterious addition of silver nanoparticles [11]. Nabil et al. [12] reported the TC enhancement for TiO<sub>2</sub>-SiO<sub>2</sub> based NFs (ethylene glycol base fluid) with increase in both nanoparticles volume concentration and temperature. Few more studies have also revealed the heat transfer and viscosity benefits of the TiO<sub>2</sub>-SiO<sub>2</sub> based NFs [13,14]. Studies on TiO<sub>2</sub>-Al<sub>2</sub>O<sub>3</sub> NFs informed that the TC enhancement ranges between 15.3 and 19.2% which is higher than 8.5–17.7% for simple alumina NF, and from 10.7 to 14.1% for titania NFs, [15]. Studies on TiO<sub>2</sub>-CuO/water hybrid NFs informed better thermal performance relative to its mono-NF [9]. The TiO<sub>2</sub> based hybrid NF used in a tubular heat exchanger revealed 30.4% increase in overall heat transfer for a volume concentration of 0.7% [16].

It is to be noted that thermal properties of fluids are strongly dependent on the size and shape of the suspending nanoparticles, and could be explained in terms of shape factor of NPs [17,18]. Graphene (a two-dimensional (2D) honeycomb carbon lattice) and related carbon nanostructured materials are known to have a high TC (~5000 W/m.K), a large surface area, high mechanical strength, and a low density, proving their suitability for heat transfer improvements in hybrid NF formulations [19]. The synergetic effect TiO<sub>2</sub> and graphene NP have been notified through the rheological and machining characteristics in biodegradable vegetable oil based NF [20]. The TiO<sub>2</sub>-graphene hybrid NFs in water showed a long-time dispersion stability and a significant enhancement (33%) in the TC at the concentration of 0.1 wt% (0.078 vol%) [21]. Functionalized graphene and doped graphene exhibited beneficial properties for composite formation and improvement in dispersion [22–25]. Recently, another heteroatom included graphene, graphitic carbon nitride (g-C<sub>3</sub>N<sub>4</sub>, GCN), received greater attention by researchers in various areas due to their low bandgap energy, excellent visible light absorption, catalytic, photocatalytic properties and other physiochemical merits [26]. The GCN combined heterojunction with TiO<sub>2</sub> exhibited enhanced absorption of visible light and photocatalytic performance for hydrogen production [27]. GCN based hybrids have proved to show synergistic effects and improved properties for various applications [28,29]. Similar studies on TiO<sub>2</sub>/GCN for other application trigger interest on such materials.

Studies on two solid particles dispersed hybrid NFs motivated the researchers to explore much more improved thermo physical characteristics with the inclusion of additional nanoparticles in the NFs and this triggers the researches to develop tri-hybrid NFs (THNF) by dispersing three solid nanoparticles suspended in a base fluid. Mingyan et al. [30] reported improved stability and thermal performance of the Al<sub>2</sub>O<sub>3</sub>-TiO<sub>2</sub>-Cu/Water THNF as compared to the mono nanofluid. Zayan et al. [31] explained the rheological behaviour of the GO-TiO<sub>2</sub>-Ag/water THNF in terms of energy transfer phenomena. Sadaf et al. [32] reported the NPs revealed the importance of THNF on new unique by selecting blood as base fluid and with different kind of suspended. Further, THNFs were prepared with different shaped nanometer sized solid particles [33] and exhibited better stability and thermal properties [34–36] over the individual NPs based NFs. The CuO/TiO<sub>2</sub>/SiO<sub>2</sub> THNFs were formulated and found to exhibit increased temperature output at higher solar radiations with a maximum temperature output at 73 °C under 700 W/m<sup>2</sup> [37]. Another report on THNF focused on thermo-hydraulic and exergetic analysis using different shaped (spherical (Al<sub>2</sub>O<sub>3</sub>), cylindrical (CNT), and platelet (Graphene) NPs [38]. It should be noted the uses of THs are progressively increasing for various applications, there are few reports available on the studies related to TH based NFs. Though there are plenty of choices for the selection of individual nanoparticles for the preparation of TH, the selection of appropriate nanoparticles and easier synthetic procedure for the preparation of TH, is highly demanding.

Considering the importance of beneficial properties of TiO<sub>2</sub>, ZnO and GCN and absence of studies on NFs based on TiO<sub>2</sub>, ZnO and GCN as ternary suspended solid particles, we report the formulation of the new THNF and their thermophysical properties. In general, literature presents complicated, multistage, time consuming methodologies for the preparation of THs based on TiO<sub>2</sub> and ZnO. In such cases, the final products of THs were found to have uncontrolled compositions of the components and hence found difficulty in preparing THs with defined compositions. The present work utilizes a simple two stage methodology (Scheme 1) for the preparation of

proposed TH, which provides advantages and superiority in terms of ease of preparation and quantitative product generation. In the first stage, we prepared GCN through a green hydrothermal synthesis involving the natural and inexpensive glucosamine as the precursor (Scheme 1). The second stage involves the simple mixing of ZnO and TiO<sub>2</sub> with GCN at an elevated temperatures using calcination. (Scheme 1). The demonstrated methodology is superior considering the often reported complicated, multistage and time consuming processes for the preparation of TH. The present work reports the new THNF formulation based on TH comprised of TiO<sub>2</sub>, ZnO and GCN (designated as TZG) in various compositions of the component material and their thermophysical properties for the first time.

## 2. Experimental details

### 2.1. Chemicals

The chemicals, N-Acetyl D-Glucosamine (C<sub>8</sub>H<sub>15</sub>NO<sub>6</sub>) (extrapure AR grade 99% powder SRL India), TiO<sub>2</sub>nanopowder (average particle size is 30–50 nm (diameter), purity 99.9% spherical morphology and density 4.01 g/cm<sup>3</sup>)(Nano Research Lab, India)and ZnO nanopowder (average particle size is 30–50 nm, purity 99.9%, spherical morphology and density 6 g/cm<sup>3</sup>) (Nano Research Lab, India) were purchased and used without further purification.

### 2.2. Formulation of TZG based THNF in EG: water base fluid

The formulation of TZG based THNF involves three stages that include; i) preparation of GCN, ii) preparation of TZG TH and iii) preparation of THNF.

#### 2.2.1. Preparation of GCN

GCN was prepared using C<sub>8</sub>H<sub>15</sub>NO<sub>6</sub> (the carbon and nitrogen source) by adopting a similar procedure available in literature [39] and subsequently included with an additional step as calcination of the product obtained in the literature procedure [43] (Scheme 1). Typically, about 5 gm of C<sub>8</sub>H<sub>15</sub>NO<sub>6</sub> was dispersed in 100 mL deionized (DI) water in a porcelain crucible, evaporated the water at 80 C to obtain a paste and then transferred the pasty mass into a Teflon sealed autoclave tube. Upon heat treatment at 140C for 12 h, a yellow mass was obtained. In the second thermal treatment step, the yellow mass was calcined at 550 °C for 4h to get a black coloured powder. The procedure is described in Scheme 1. The first stage product [39] is graphitised to result GCN in the second step high temperature calcination.

#### 2.2.2. Preparation of TZG TH

Calculated quantities of TiO<sub>2</sub> and ZnO were mechanically mixed in a mortar with pestle and subsequently calcined at 500 C (Scheme 1). THs with various compositions were prepared by varying the mass ratios of TiO<sub>2</sub> and ZnO with a constant mass(0.12 g) loading of GCN. Typically, TiO<sub>2</sub> and ZnO mass ratios were varied as 1:0.2, 1:0.5, 1:0.8, 0.2:1 and 0.5:1.0 and GCN was kept as constant mass for the preparation of TZG TH and the THs were designated as TZG TH1, TZG TH2, TZG TH3, TZG TH4 and TZG TH5, respectively. Binary hybrids, TiO<sub>2</sub>+GCN and ZnO\_GC\_N were also prepared for comparison purposes.



Scheme 1. Preparation of TZG THNCs.

### 2.2.3. Preparation of TZG based THNF (TZG-THNF)

The 0.5% concentration TZG THNF in EG: water (60:40 v/v) was prepared by dispersing the TZG TH in the base fluid under sonication at room temperature. The quick settlement of nanoparticles is the extremely unwanted problem for various hands-on heat transfer/cooling applications. The TZG TH NPs were suspended stably through long time (30 min) s stirring.

### 2.3. Characterization of TZG-TH and determination of thermophysical properties of TZG-THNF

Morphology and elemental analysis were carried out using Scanning Electron microscope (Zeiss EVO LS 15 instrument. TEM images are recorded on JEOL JEM 2100 instrument at PSG institute of advanced studies. XPS spectra was collected on Kratos Axis Multi-technique X-ray Photoelectron Spectroscopy system at CENSE, Bangalore.

The ultrasonic velocity measurements were carried out using Digital ultrasonic velocity meter (VI MICROSYSTEMS make, 2 MHz, VCT-70A model, accuracy:  $\pm 0.001$  m/s) at 303K. The viscosity of the TZG-TH suspensions was determined for at 303K by a Digital Viscometer (BROOKFIELD make, USA, accuracy:  $\pm 0.01$  cP). Pyknometric method is employed to determine the density of the TZG-THNF. A K-ROY make electronic balance having an accuracy of  $\pm 0.001$  gm is used to measure the mass of the liquid. The Abbe refractometer double prism system (MITTAL make) with monochromatic light source (Sodium vapour lamp) of 589 nm for

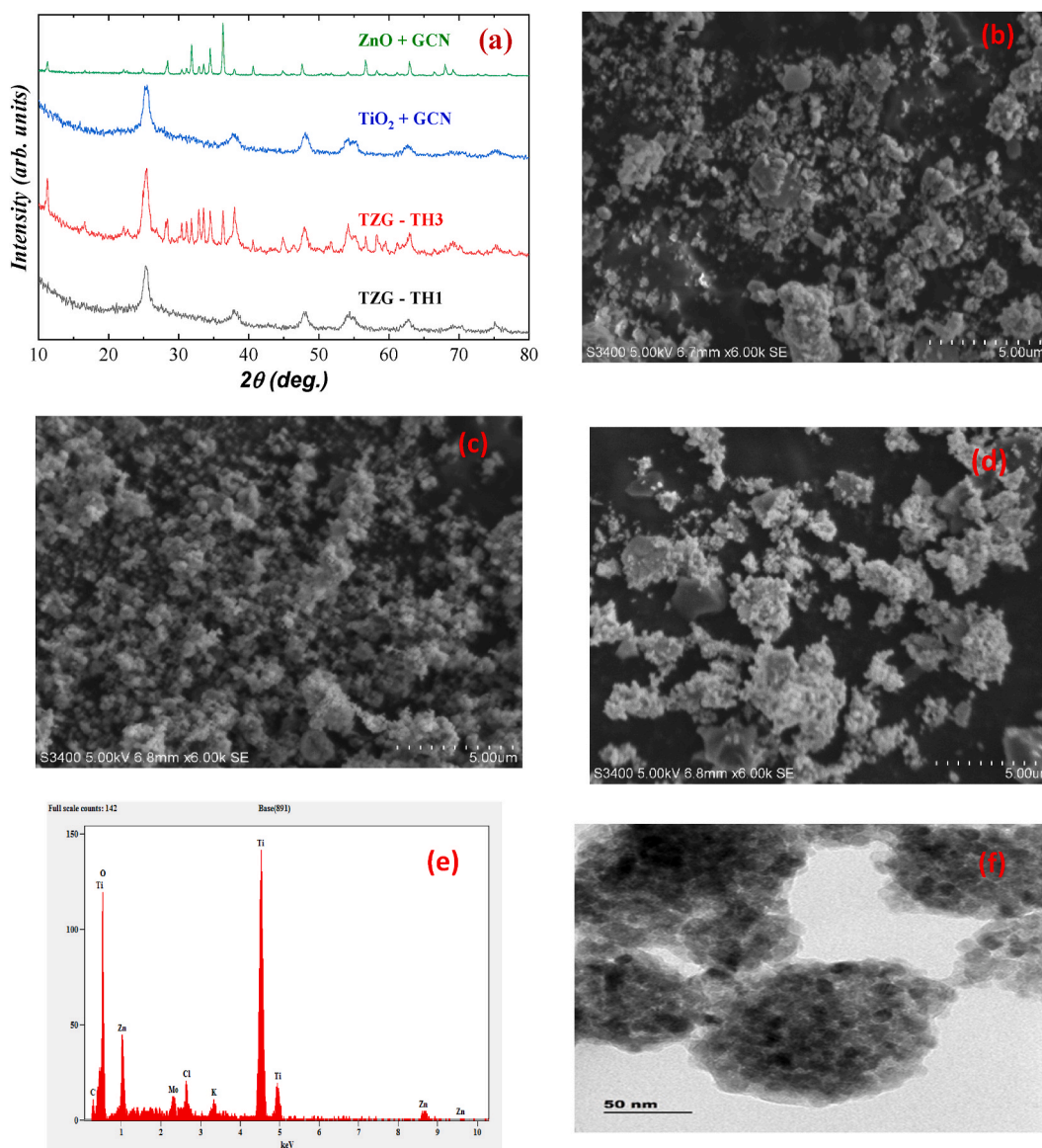


**Fig. 1.** (a) XRD pattern of TZG TH1, TZG TH3, TiO<sub>2</sub>+GCN and ZnO + GCN. SEM images of (b) TZG TH1 c) TiO<sub>2</sub> (annealed at 550 C), (d) ZnO (annealed at 550 C) and e) EDS of TZG TH1 and f) HRTEM image of TZG-TH1.

illumination and with accuracy of  $\pm 0.001$  was used for measuring the refractive indices. An electronically controlled thermostat with a temperature measuring accuracy of  $\pm 0.05$  K was used to circulate water at 303 K during the measurement of the properties of NFs using viscometer, interferometer, refractometer and density measurements. The zeta potential values were measured using the Zetasizer (Litesizer 500, Malvern Pananalytical Ltd., Malvern, UK) instrument. The details of calculating the thermal conductivity and molecular interaction parameters like adiabatic compressibility, intermolecular free length, free volume, internal pressure and specific acoustic impedance are presented in supporting information (SI-1 and SI-2)

### 3. Results and discussions

#### 3.1. Structure, Morphology and microstructure of TZG-TH

Fig. 1a presents the XRD patterns of the TZG-TH1 and TZG-TH3 containing fixed amount of  $\text{TiO}_2$  and different amount of ZnO. The XRD pattern exhibits  $2\theta$  peaks of anatase titania (JCPDS no. 21–1272) and hexagonal phase wurtzite structure (JCPDS number 80–0074) of ZnO. The XRD pattern of TZG-TH1 and TZG-TH3 did not show the intense peak in the region of  $27.4^\circ$  that is associated

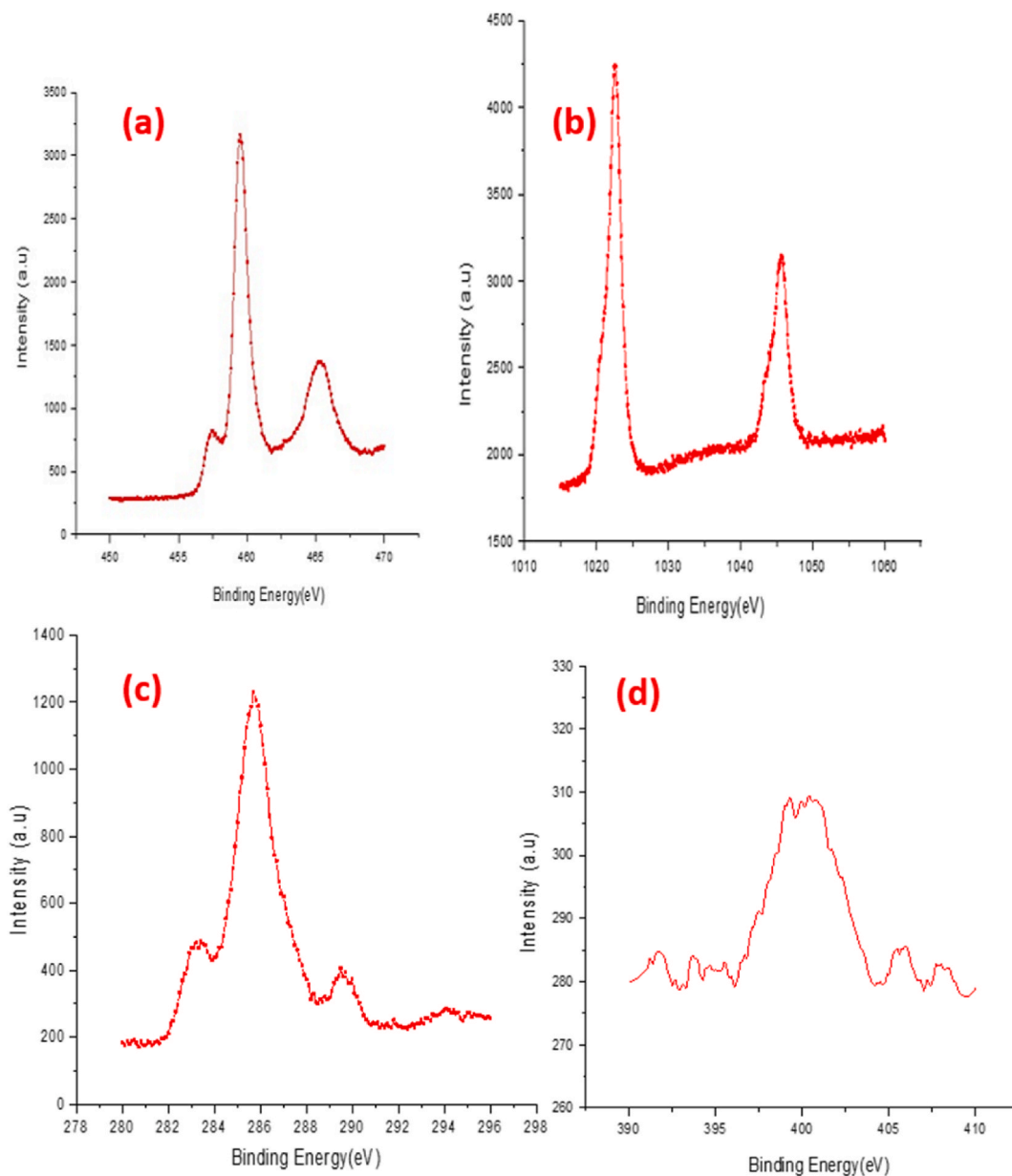


Fig. 2. XPS core level spectrum of (a) Ti 2p, (b) Zn 2p, (c) C 1s and (d) N 1s elements of TZG-TH1.

with the characteristic interlayer stacking of conjugated aromatic ring in GCN due to overlapping with anatase peak at similar 2 $\theta$  position. To note, the peak positions of taitania and wurtzite remain the same in TZG-TH1 and TZG-TH3 indicating that increase in amount of one component with respect to other did not influence the crystal structure. To understand the influence of GCN on influencing the crystal structure of TiO<sub>2</sub> or ZnO, the XRD patterns of TiO<sub>2</sub> + GCN and ZnO + GCN were recorded. We noticed that the peak positions of TiO<sub>2</sub> or ZnO are not influenced by the inclusion of GCN in TH. The microstructure of the TZG is inferred through a comparison of scanning electron microscopy (SEM) images of a typical TH, namely TZG-TH1 (Fig. 1b) with pure TiO<sub>2</sub> (Fig. 1c) and ZnO (Fig. 1d). The SEM image TZG TH1 informs that the nanolayers are randomly filled with metal oxide NPs and looking as agglomerated particles having a friable structure (Fig. 1b). The SEM image of 550 C annealed TiO<sub>2</sub> shows the scattered presence of random sized spherical TiO<sub>2</sub> NPs. (Fig. 1b). SEM image of 550 C annealed ZnO shows the presence of particles with larger agglomeration as compared to TiO<sub>2</sub> particles. The EDS of TZG-TH 1 shows the presence of Ti, Zn, O and C as main elements (Fig. 1e) along with deleterious presence of impurity elements (K, Cl) as evident from the very low atomic %.

High resolution transmission electron microscopy (HRTEM) image of TZG-TH1 is shown in Fig. 1f. HRTEM image clearly shows the presence of narrowly distributed smaller sized spherical particles having the average sizes in the range 40 nm–90 nm in sheet like structure.

Fig. 2 presents the XPS core level spectrum of important elements (Ti, Zn, C and N) in TZG-TH1. Fig. 2 informs the presence of characteristic peaks at 463.8 and 458.0 eV that correspond to the Ti<sup>4+</sup> 2p<sub>1/2</sub> and Ti<sup>4+</sup> 2p<sub>3/2</sub> groups in TiO<sub>2</sub>, peaks at 1025.0 and 1042.0 eV of Zn 2p<sub>3/2</sub> and Zn 1/2 electronic states, peaks at 286 eV and 290 eV that arise from the surface adventitious C and sp<sup>2</sup>-bonded C in the C=N coordination bond (that can exist in GCN), respectively (Fig. 4a) and three main peaks at around 398.2 eV (pyridinic-N), at 391.2 eV, (pyrrolic-N/Cu-N) and 401.5 eV (graphitic-N) which are the main features of GCN. The elemental composition and electronic states of elements clearly confirm the formation TZG -TH.

### 3.2. Thermophysical properties of TZG-THs

#### 3.2.1. Viscosity

The experimental measurement of viscosity is very much important as it is closely associated with the thermo-fluidic behaviour of heat transfer fluids. Besides, few other parameters of heat transfer-based engines such as pumping power, pressure drop and convective heat transfer can be directly inferred by knowing the viscosity of fluids [40–43]. In the literature, the effects of temperature, particle size and volume concentration on viscosity of NFs are prevalently available [44–46]. The effect of nanoparticle concentration, size, surfactants, temperature, base fluid, nanoparticle shape and material on viscosity has been given attention [47]. The increasing trend of viscosity is correlated to higher suspension concentration of the NPs in base fluid, causing higher internal viscous shear stresses reported by some other researchers [48,49]. There are limited number of reports available on the viscosity of few TiO<sub>2</sub>, ZnO and carbon nanostructures based binary hybrid materials. However, the viscosity of ternary hybrid materials-based NFs are rare in literature.

In the present work, viscosity of TZG TH based NF (Fig. 3) was found to show a non-linear variation with the composition of TiO<sub>2</sub>, ZnO and GCN. Fig. 3 informs that viscosity of ZnO + GCN containing NF (3.62 cP) is slightly higher than base fluid (3.5 cP) but lower than GCN (3.79 cP). However, viscosity of TiO<sub>2</sub>+GCN (~4.1 cP) is higher than GCN or base fluid. Typically, the viscosity values of TZG TH1, TZG TH2, TZG TH3, TZG TH4 and TZG TH5 are higher than ZnO + GCN based NF and and lower than TiO<sub>2</sub>+GCN based NFs. While the decrease in viscosity with respect to TiO<sub>2</sub>+GCN for the TZG-THs is marginal (from 4.1 cP to 3.90), the increase with respect to ZnO + GCN is significant (renaming from 3.62 cP to 3.95 cP). Typically, TZG TH5 containing larger proportions of ZnO showed 9.11 % higher increase in viscosity with respect to ZnO + GCN and 12.1 % increase than base fluid. It is presumed that pronounced increase or decrease in viscosity with composition of mixed materials indicates the presence of particle interactions between the either of the components and the base fluid due to the larger surface area of nanoparticles. For similar concentration of single material and hybrids, the viscosity of hybrid-based NFs would be more significant as compared to the base fluid and the individual single material of the

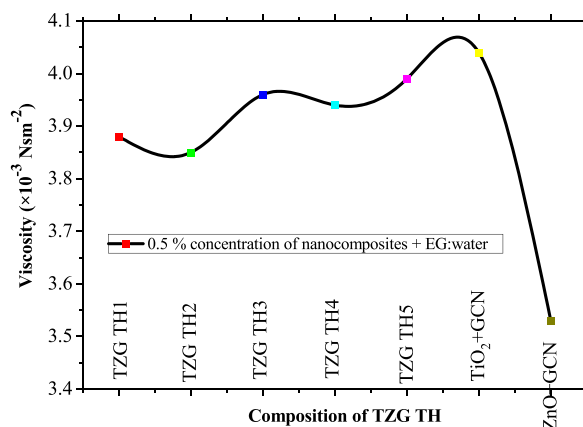


Fig. 3. Variation of viscosity against composition of TZG TH.

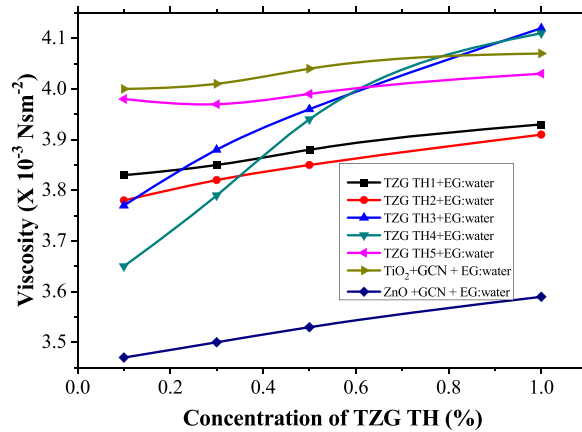


Fig. 4. Variation of viscosity against concentration of TZG TH based NFs.

hybrid [50]. It is important to note that most of the reports on TH based NFs discussed the effects of particle concentration, temperature, and particle size on the viscosity of THNFs. The studies on the viscosity of Al<sub>2</sub>O<sub>3</sub>/CuO/TiO<sub>2</sub> based THNF informed the volume fraction (0.01–0.1%) and temperature (35 °C–50 °C) [35]. The results on viscosity revealed an increase with the solid volume fractions and decrease with increasing temperature. Interestingly, the maximum enhancement of viscosity of 55.41% and 17.25% has been witnessed for 0.1% vol. fraction of THNF as compared to binary Al<sub>2</sub>O<sub>3</sub>–TiO<sub>2</sub> and Al<sub>2</sub>O<sub>3</sub>–CuO hybrid NFs. In another report on THNF, the viscosity change has been predicted due to the cluster formation and internal viscous stress on the base fluid upon addition of nanoparticles [51]. Studies on viscosity of Al<sub>2</sub>O<sub>3</sub>/TiO<sub>2</sub>–ZnO THNF informed increase with volume fraction [52]. The increased viscosity of water-based Al<sub>2</sub>O<sub>3</sub>/SiC/TiO<sub>2</sub> THNF was notified with increase in volume fraction of solid particles and explained in terms of more mixing of the layers in the base fluid [35]. The results on CuO/TiO<sub>2</sub>/SiO<sub>2</sub> THNF informed that the decrease in viscosity with increasing temperature, and the increase with increasing volume fraction [53]. The report on the viscosity of Cu/SiO<sub>2</sub>/MWCNT/water THNF informed a Newtonian behavior and the viscosity of THNF showed increase possibly due to the increase in the number of NPs [54]. The observed non-linear trend with the composition of TZG THF in this work could not be explained with the increase in number of NPs, but presumably due to the difference in hybridization effect with the variations in the composition of TZG THF. Typically, TZG TH5 shows the highest viscosity ( $4.4 \times 10^{-3} \text{ Nsm}^{-2}$ ) for 1.0% mass concentration of TZG TH. Fig. 4 informs that the viscosity increases nearly linearly with increase in concentration for all TZG THNFs (0.1–1.0% mass concentration). Here again, one can notice that TZG THs show lower viscosity values for any concentration in comparison to TiO<sub>2</sub>+GCN based NFs and higher than ZnO + GCN based NFs. The increasing tendency of viscosity can be attributed to higher suspension concentration of the NPs of the THs in base fluid, causing higher internal viscous shear stresses [48,49]. Fig. 4 informs the general trend that ZnO in rich proportion based NFs have far lesser viscosity at any concentration than TiO<sub>2</sub> in higher proportion based NFs. concentration range 0.1–0.8 % mass concentrations.

### 3.2.2. Density

Effective density is an important property for a NF and it is related to the effectiveness in heat transfer applications. Density influences the Nusselt number, friction factor, and Reynolds number [55]. Literature reveal that the density of NF is influenced by temperature, volume fraction of nanoparticles, base fluid density and the ratio of base-fluid to nanoparticles [56,57]. In the case of

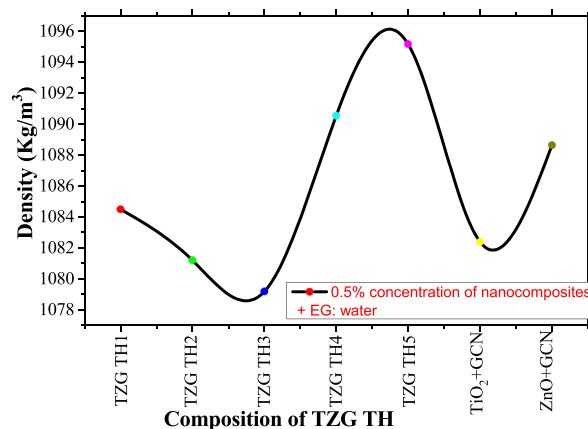


Fig. 5. Variation of density against composition of TZG TH.

two-phase mixtures based NFs, the density was correlated in terms of slurry [56], density of NP, density of base fluid and concentration of solid particle per unit volume. With regards to the prediction of density of NFs, the generally used mixture rule predicts over-estimated NF density values. There can be deviation from the theoretical and experimental density of NFs and the deviation was explained in terms of nanolayer formation. It has been considered that NF is a three-component multiphase system comprising of NPs as solid, base fluid as liquid and nanolayer as a solid-liquid interface [57]. However, the density correlation in THNF is not straight forward as it contains many kinds of NPs.

In the present study, on the first look at the density results on TZG THs (Fig. 5), prepared with varying compositions of  $\text{TiO}_2$  and ZnO, it can be inferred that density shows a non-linear variation with composition of TZG TH. Keeping note of the density values of the various components,  $\text{TiO}_2$  (4.02 cP), ZnO (5.61 cP), and GCN (2.34 cP) as well the base fluid (1.060 cP), we interpret the changes in density with composition of TZG THs. The density of TZG TH varies from 1.079 to 1.095 cp, which is not much higher than the base fluid. The TZG TH4 and TZG TH5 (having higher proportion of ZnO in TH) have higher density values than the binary composites based NFs,  $\text{TiO}_2$ +GCN (1.083 cP) and ZnO (1.087 cP). The TZG TH2 and TZG TH3 (prepared with higher proportion of  $\text{TiO}_2$ ) have lower density values as compared to binary composites ( $\text{TiO}_2$ +GCN and ZnO (cP) included NFs. The noticeable increase or decrease in density with composition of TZG THs indicates the presence of possible interactions between the component particles in TZG and base fluid. Fig. 6 shows the variation of density with concentration for the individual TZG TH. The general trend that is noticeable for all the THs is that the density value is minimum at lower concentration (0.1%) and maximum at higher concentration (1.0%). The increase in density with concentration of TZG TH in NF for any of the TZG TH is correlated to the increase in number of particles and hence increase in interactions between the component particle of TZG THs and base fluid. It is to be noted that increase in concentration can cause increase in the number of nanoparticles. The influence of particle sizes of any of the TH on density can be considered negligible because of the existence of similar sized particles. Amongst the TZG THs based NFs, the density of TZG TH-5 is highest for the entire concentration range (0.1–1.0 %) amongst the TZG THs. The trend in viscosity and density for TZG TH-5 corroborates each other in the NF.

### 3.3. Ultrasonic velocity

Measurement of ultrasonic velocity for a solvent/solution plays a useful role in understanding the physico-chemical behavior of solvent/solution. The ultrasonic velocity measurement is helpful in the calculation of few important thermodynamic properties which provide qualitative information regarding molecular interactions [48,58–60]. In this work, the ultrasonic velocity of the TZG TH based NFs is higher as compared to their binary counter parts,  $\text{TiO}_2$ +GCN and ZnO + GCN based NFs (Fig. 7). It is to be noticed that the ultrasonic velocity has non-linear variation with changes in the composition of TZG TH in the NFs. The ultrasonic velocity values of TZG THs are much higher than ZnO + GCN and marginally higher than  $\text{TiO}_2$ +GCN based NFs. However, one must notice from Fig. 5 that the ultrasonic velocity of TZG TH-3 is deplorably lower than the other TZG THs. The pronounced increase or decrease in these thermo-physical parameters with composition of mixtures indicates the presence of interactions between the components of TZG THs and the base fluid. This could result in dipole-dipole interaction or hydrogen bonded complex formation between unlike molecules [50]. While molecular interactions could be assigned as the reason for the changes in ultrasonic velocity, it is difficult to clearly demonstrate the influence of individual component of the TH on ultrasonic velocity changes.

Fig. 8 presents the variation of ultrasonic velocity with concentration of the TZG THs in the NFs. The ultrasonic velocity shows linear variation with increase in concentration of TZG THs in the NFs (Fig. 6). In general, increasing trend in ultrasonic velocity than the base fluid suggests that there can be considerable occurrence of structural reorganization of the NPs in the base liquid leading to the weakening of intermolecular forces. The increase in ultrasonic velocity in NF may also be due to surface effect that arises from the possible hydrogen bonding interactions between solid particles and water molecules in the NF [61]. Fig. 8 informs that the increase in ultrasonic velocity is minimum with ZnO + GCN. The density results with ZnO + GCN give a clue that the influence of ZnO on density may be minimum (Fig. 5 and 6). The increase in random movements of NPs with increase in concentration and when the ultrasonic

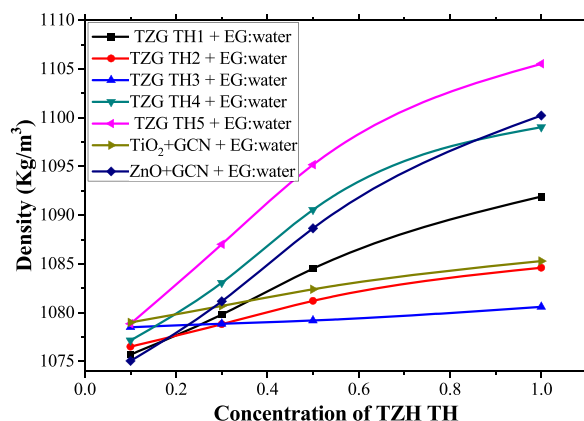


Fig. 6. Variation of density against concentration of TZG TH based NFs.

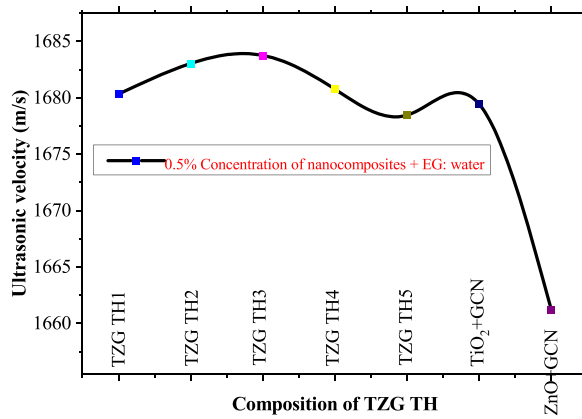


Fig. 7. Variation of ultrasonic velocity against composition of nanocomposites.

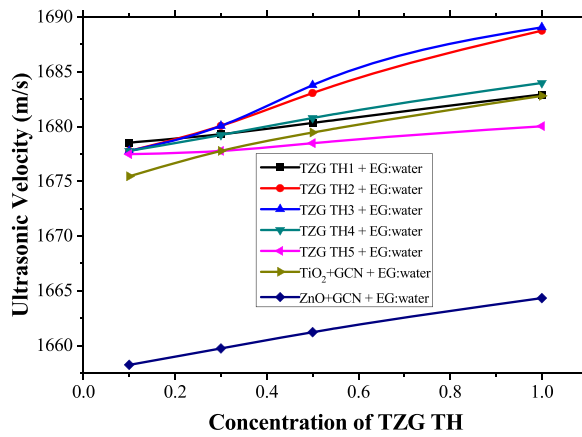


Fig. 8. Variation of ultrasonic velocity against concentration of TZG TH based NFs.

vibration is propagated in NF. The decrease in ultrasonic velocity is ascribed to the stopping of Brownian motion of the particles in suspension. This indicates that there can be deviation in the trend in ultrasonic velocity with concentration. Also, agglomeration of particles leads to collisions between the suspended particles [62]. Similar results are reported by Yadav et al. [63].

In a report on the TiO<sub>2</sub> + Fe<sub>2</sub>O<sub>3</sub>+SiO<sub>2</sub> TH based NF in water: EG, the velocity variation with the components in TH was discussed through nonlinear systems via Newton built-in-shooting technique [64]. Though few theoretical interpretations on velocity related parameters of THNFs are available [65,66], experimental investigations are very rare.

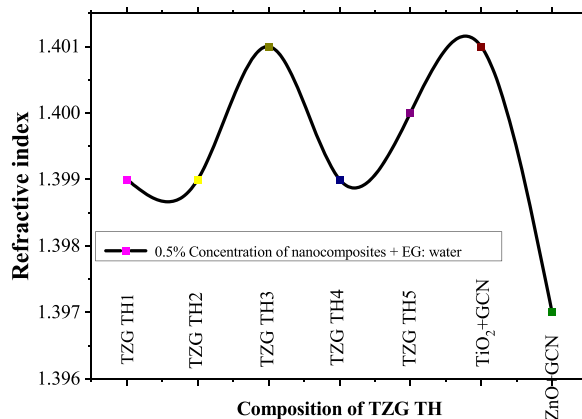


Fig. 9. Variation of refractive index against composition of nanocomposites.

### 3.4. Refractive index

The refractive index (RI) indicates the interaction between light and particles [67]. Despite the availability of the studies on thermophysical properties of few of the THs containing NFs, there is lack of information about their experimental investigation on the studies on the optical properties of THNFs. In this work, the variation of RI with the compositions of TZG TH in the THNF is investigated. Fig. 9 informs that RI has non-linear variation with the composition of TZG TH. Our results inform that the RI values of TZG TH1, TZG TH2, TZG TH3, TZG TH4, TZG TH5 are lower as compared to RI of TiO<sub>2</sub>+GCN based binary fluids and higher than ZnO + GCN based binary NFs. It is known that TiO<sub>2</sub> has high refractive index (RI = 2.45 and 2.7 for anatase and rutile phase, respectively). And, the RI of pure ZnO ranges from 1.78 to 1.48 in the wavelength range of 300–900 nm. The RI of GCN is 2.54, The RI of the base fluid is 1.425. Keeping these RI values into account, the RI values of the TZG -THs studied in this investigation are lower than the solid components, and base fluid. Also, the fact that RI is related to the depth of penetration of the incident photons and their absorbance during the propagation in the NFs, the lower values of RI for TZG THs suggest the lowering as possible scattering effects between the three kinds of nanoparticles and light in the NFs. The interactions with light follow non linear variation with the composition, possibly due the differences in the level of interactions between light and the individual NPs. The RI of TZG TH3 based NF is the highest (1.401) amongst the studied THNFs. The variation of RI with volume fraction of -Al<sub>2</sub>O<sub>3</sub>, SiO, TiO<sub>2</sub>, and-Al<sub>2</sub>O<sub>3</sub> based NFs has been reported with volume fraction of NPs [68]. The absence of increase in RI for the THs indicates the lesser extent of aggregation effects [68]. There are reports on the details of theoretical perspective of optical properties of NFs [69].

The RI values of the TZG THs ncluded THNFs, TiO<sub>2</sub>+ GCN and ZNO + GCN included binary NFs are reported in the concentration range of 0.1%–1.0% at 303K (Fig. 10). A general trend is observed for the TZG THs included NFs. The RI increases with increase in concentration of TZG THs in the NFs.

### 3.5. Thermal conductivity

TC is essential for understanding the heat transfer characteristics of a NF. Fig. 11 presents the TC values of NFs included with TZG TH having compositional variatioss and also for the binary ZnO + GCN, TiO<sub>2</sub>+GCN based NFs. TCs of TZG TH included NFs show non-linear variation with composition of TZG THs. The TC enhancements of ZnO + GCN and TiO<sub>2</sub>+GCN included NFs are 206 % and 208%, respectively, as comapred to the TC of base fluid. The TC enhancements of ZnO + GCN and TiO<sub>2</sub>+GCN are much higher than ZnO mono NF (26.9%) [70] and TiO<sub>2</sub> mono NF (33.0%) [71] The TC enhancementsof TZG-THs, studied in the work, are slightly higher (~210%) than TC enhancements of ZnO + GCN and TiO<sub>2</sub>+GCN, Typically. TC is maximum for TZG TH5 (prepared with higher propostions of ZnO) based THNF (53.137 W/m/K)

Fig. 12 presents the TC changes of individual TZG TH based NFs for various concentrations. Irrespective of the composition of the TiO<sub>2</sub> and ZnO in the THs, TC showed an increasing trend with increase in concentration of TZG TH. A similar trend has been notified on CuO/-TiO<sub>2</sub>/SiO<sub>2</sub> THNF with various compositions of TH [57]. ZnO + GCN based NF exhibited lowest TC as comapred to TZG THs and TiO<sub>2</sub>.GCN based NF. Here again, ZnO based NFs show the lowest thermal conductivity in all tested concentrations of TZG THs as well to pure TiO<sub>2</sub> based NFs. The TC increase with the increase in concentration is explained due to the increase in Brownian motion of suspended NPs [72,73]. The TC changes of Mn<sub>0.5</sub>Zn<sub>0.5</sub>Fe<sub>2</sub>O<sub>4</sub> TH were reported for varying volume fraction of the particles in the NFs and a 45% TC enhancement at 10% volume concentration was notified [74]. The heat absorption efficiency of CuO/TiO<sub>2</sub>/SiO<sub>2</sub> THNF was investigated under solar radiation for different concentrations [37]. TheTC changes of MWCNT-TiO<sub>2</sub>-ZnO THNF have been reported over volume fraction of 0.1%–0.45% [75]. TC variation of Cu/SiO<sub>2</sub>/MWCNT/water THNF was investigated for various volume concentration (1–3%) ranges and the increase in TC with concentration was explained in terms of the Brownian motion changes [54].

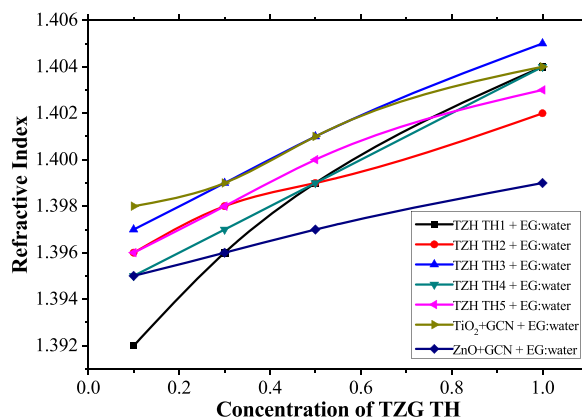


Fig. 10. Variation of refractive index against concentration of TZG TH based NFs.

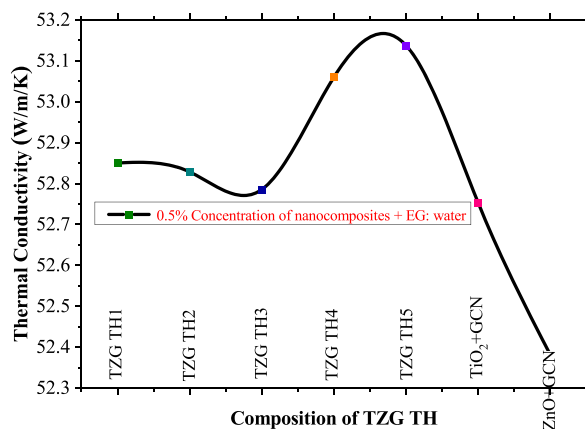


Fig. 11. Variation of thermal conductivity with composition of hybrids included NFs.

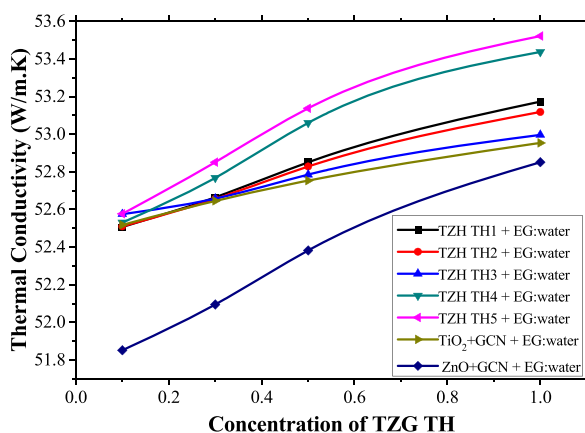


Fig. 12. Variation of thermal conductivity against concentration of TZG TH based NFs.

### 3.6. Molecular interaction properties

The experimental values of ultrasonic velocity, viscosity and density of TZG THs based THNFs are used to deduce molecular interaction parameters like adiabatic compressibility ( $\beta$ ), intermolecular free length, free volume, internal pressure and specific acoustic impedance ( $Z$ ) [48]. (Table 1). The calculation method of the parameters are detailed in SI 2. The  $\beta$  value indicates the molecular interactions in NFs. The decreasing trend of  $\beta$  with increase in concentration of the solid particles gives the information regarding the associations or disassociation of the components and packing of particles [76,77]. The variation of  $\beta$  for TZG THs based THNFs is presented in Table 1. For any of the selected TZG TH based NF, the  $\beta$  value shows a non-linear trend with composition of TZG TH in the NF. The observed non-linear trend in  $\beta$  with composition of TH as well with concentration is an evidence of existence of intra/inter particles interactions between the component particles and the molecules of base fluid. A similar kind of non-linear trend is observed for the influence of concentration of NF on intermolecular free length. We envisage the possible interaction between particles of TZG THs and base fluids, which may lead to structural reorganizations in the liquid system. Free volume refers to the void space between the molecules, i.e., the volume present as holes because of irregular packing of the molecules. It is defined as the average volume in which the central molecule moves freely inside the hypothetical cell without being affected by the repulsion of surrounding molecules. The free volume values with composition of TZG THs follow a reverse trend noticed with respect to the influence on viscosity (Table 1). This indicates that viscosity rather than velocity determines the free volume of our system. The free volume reduces when the internal pressure increases [78]. The reverse trend of free volume with internal pressure is clearly observed in Table 1. The  $Z$  refers to the impedance offered to the sound wave by the components of the TH. Mathematically,  $Z$  is directly proportional to ultrasonic velocity and inversely proportional to ( $\beta$ ). Table 1 informs a non-linear variation of specific acoustic impedance with the composition of TZG THs. The non-linear decrease of  $Z$  with concentration informs that there can be molecular interactions [79,80]. The  $Z$  is maximum for TZG TH5 with a value of  $1.8036 \times 10^6 \text{ kgm}^{-2}\text{s}^{-1}$  and higher than ZnO + GCN ( $1.7899 \times 10^6 \text{ kgm}^{-2}\text{s}^{-1}$ ). The interaction between particles and base fluid molecules increases the intermolecular distance between the molecules which in turn causes increase in  $Z$  [81]. The relaxation time increases with increasing concentration of TZG THs. This indicates that molecular interaction may be stronger at higher concentrations. Surface tension is a force between molecules that develops at the interface between two immiscible

**Table 1**  
Various Molecular interaction parameters at 303K

Name of the sample	Concentration (%)	Adiabatic Compressibility ( $\beta$ ) ( $\times 10^{-10} \text{ m}^2 \text{ N}^{-1}$ )	Intermolecular free length ( $\times 10^{-11} \text{ m}$ )	Free volume ( $\times 10^{-9} \text{ m}^3 \text{ mol}^{-1}$ )	Internal Pressure ( $\times 10^9 \text{ Pa}$ )	Specific acoustical impedance ( $\times 10^6 \text{ kg m}^{-2} \text{ s}^{-1}$ )	Relaxation time ( $\times 10^{-12} \text{ s}$ )	Surface tension (N/m)
TZG TH1	0.10	3.300	3.769	6.032	2.803	1.805	1.685	45.32
	0.25	3.284	3.760	5.989	2.816	1.813	1.686	45.35
	0.50	3.266	3.749	5.925	2.835	1.822	1.689	45.39
	0.75	3.251	3.741	5.886	2.847	1.829	1.691	45.44
	1.00	3.234	3.731	5.826	2.864	1.837	1.694	45.50
TZG TH2	0.10	3.300	3.769	6.148	2.786	1.806	1.663	45.29
	0.25	3.284	3.760	6.064	2.803	1.812	1.672	45.38
	0.50	3.265	3.749	6.009	2.816	1.819	1.676	45.50
	0.75	3.248	3.739	5.957	2.827	1.825	1.680	45.63
	1.00	3.233	3.730	5.901	2.839	1.83	1.685	45.73
TZG TH3	0.10	3.294	3.765	6.172	2.786	1.809	1.656	45.29
	0.25	3.284	3.760	5.924	2.825	1.812	1.698	45.38
	0.50	3.268	3.751	5.764	2.851	1.817	1.725	45.53
	0.75	3.258	3.745	5.585	2.883	1.820	1.759	45.62
	1.00	3.244	3.737	5.457	2.906	1.825	1.781	45.74
TZG TH4	0.10	3.298	3.768	6.479	2.739	1.807	1.605	45.28
	0.25	3.274	3.754	6.132	2.800	1.818	1.654	45.35
	0.50	3.246	3.738	5.793	2.867	1.832	1.705	45.41
	0.75	3.226	3.726	5.586	2.910	1.842	1.737	45.47
	1.00	3.209	3.716	5.453	2.940	1.850	1.758	45.54
TZG TH5	0.10	3.294	3.766	5.689	2.863	1.809	1.748	45.27
	0.25	3.268	3.751	5.712	2.874	1.823	1.729	45.29
	0.50	3.241	3.735	5.672	2.895	1.838	1.724	45.32
	0.75	3.222	3.724	5.635	2.910	1.847	1.722	45.36
	1.00	3.205	3.714	5.596	2.926	1.857	1.722	45.38
TiO <sub>2</sub> +GCN	0.10	3.302	3.770	5.636	2.873	1.807	1.760	45.19
	0.25	3.287	3.762	5.627	2.877	1.813	1.758	45.29
	0.50	3.275	3.755	5.572	2.889	1.817	1.764	45.36
	0.75	3.265	3.749	5.560	2.894	1.821	1.763	45.42
	1.00	3.253	3.742	5.527	2.902	1.826	1.765	45.49
ZnO + GCN	0.10	3.382	3.816	6.868	2.683	1.782	1.565	44.50
	0.25	3.357	3.802	6.789	2.703	1.794	1.566	44.56
	0.50	3.328	3.785	6.712	2.726	1.808	1.567	44.62
	0.75	3.308	3.774	6.637	2.744	1.817	1.570	44.69
	1.00	3.281	3.758	6.563	2.766	1.831	1.571	44.74

fluids and lies on the plane of the interface. To our knowledge, studies on the surface tension of THNFs are scarce in the literature. This work reports the surface tension of TZG THs NFs over various weight concentration, of TZG THs (0.1%, 0.25, 0.5, 0.75 and 1.0%). The influence of the concentration on surface tension is shown in Table 1. The results indicate that the surface tension of TZG THs/EG:water increases with the increase of the concentration of TZG THs. The increasing surface tension with the increasing concentration of the TZG THs may be ascribed to the van der Waals forces between particles at the liquid/particle interface, which may lead to an increase of the surface free energy, resulting in the increasing of the surface tension [80].

### 3.7. Zeta potential and stability

The zeta potential ( $\xi$ ) is a crucial measure for learning more about the stability of the NF. In a colloidal suspension, the electrical potential at the slip plane between a particle's surface and a dispersion liquid is referred as  $\xi$ . Table 2 gives the stability Vs  $\xi$  relation. Table 2 informs the  $\xi$  value and the associated suspension stability of NF (for the sonication time of 30 min). The  $\xi$  value varies from 28.7 mV to 38.1 mV with 0.5 wt% NP dispersion. Table 3 presents the  $\xi$  value for the fixed concentration (0.5%) of various TZG THs. Based on Tables 3 and it is inferred that the TZG-THs have moderate stability in the NF formulation (at  $|\pm\xi| \geq 30 \text{ mV}$ ) [81–83].

UV UV-Visible spectroscopy was used to understand the dispersion stability of the prepared TZG TH based NFs. This is used because that the components of TZG TH, namely, TiO<sub>2</sub> NPs, ZnO and GCN, have high light absorption characteristics. The UV Visible spectral characteristics were followed for two of the TZH THs (TZG-TH 1 and TZG TH3) based NFs in a fixed concentration of 0.5% (Fig. 13) over the wavelength range between 190 nm and 900 nm. For comparative purposes of UV Visible spectral characteristics binary hybrids (TiO<sub>2</sub>+GCN and ZnO + GCN). The spectra of the NFs below 300 nm were noisy and hence not presented. The NFs exhibit absorbances in the waveneth region 300–900 nm without having any peaks. The absorbance changes over time were taken as the indication of dispersion stability of NFs. The absorbances of TZH THs (TZG-TH 1 and TZG TH3) based NFs showed marginal variation over longer period of standing of the NFs in a day. We believe that the moderate stability of TZH TH based NFs as witnessed by zeta potential measurement is extensible for a longer period.

Hence, we recorded the UV Visible spectra after 5 days of standing of NFs. The absorbance changes of TZH THs and the binary

**Table 2**  
Zeta potential value and associated suspension stability [80,81].

Zeta potential (+ or -mV)	Stability
0	Little or no stability
15	Some stability but settling lightly
30	Moderate stability
45	Good stability, possible settling
60	Very good stability, little settling likely

**Table 3**

Zeta Potential value for concentration (vol. 0.5%) and sonication time for (30 min).

S.No	Sample name	Zeta Potential value	Stability
1	TZG TH1	32.0 mV	Moderate stability
2	TZG TH2	30.0 mV	Moderate stability
3	TZG TH3	38.1 mV	Moderate stability
4	TZG TH4	29.0 mV	Moderate stability
5	TZG TH5	31.4 mV	Moderate stability
6	TiO <sub>2</sub> +GCN	30.1 mV	Moderate stability
7	ZnO + GCN	28.7 mV	Moderate stability

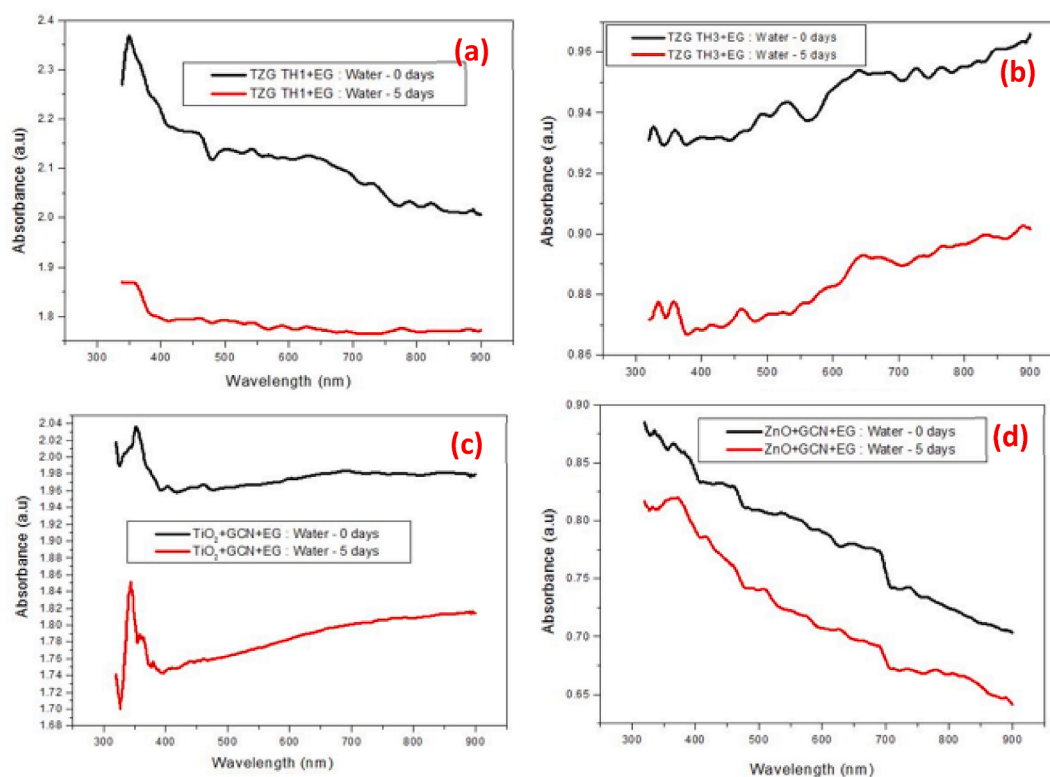


**Fig. 13.** UV Visible spectral characteristics of TZG TH included NFs: a) TZG TH1 + EG (b) TZG TH3 + EG (c) TiO<sub>2</sub> + GCN + EG and (d) ZnO + GCN + EG.

hybrid based NFs after 5 days are presented in Fig. 13. The decrease in absorbance at 500 nm (randomly selected because of the absence of specified peaks) was compared to represent the dispersion stability of the NFs. The 16.0%, 6.90%, 12.0% and 9.63% decrease in absorbance was noticed for TZG-TH 1, TZG TH3, TiO<sub>2</sub>+GCN and ZnO + GCN included NF, respectively. It is inferred that the TZG TH3 included NF has better dispersion stability than the other NFs.

#### 4. Conclusion

In conclusion, the present investigation successfully demonstrates the simple preparation of ternary (TiO<sub>2</sub>, ZnO and g-C<sub>3</sub>N<sub>4</sub>) hybrids (TH) with varying compositions of the components and the formulation of nanofluids (NFs). The influence of composition and concentration of TH in the NFs on thermophysical and molecular interaction parameters are detailed. The findings reveal the considerable enhancement in thermal conductivity (~210%) for the new TH included NF in comparison with the thermal conductivity enhancement of ZnO mono NF (26.9) and TiO<sub>2</sub> mono NF (33.0%), and binary types of NFs. The improved thermophysical properties of TH based NFs is attributed to the synergistic effects of the unique properties of the individual nanoparticles in the TH. In conjunction with the thermal conductivity enhancement, the TH included NFs exhibited advantageous properties like viscosity which suggest that the present study formulated NFs can find application wherever the cooling aspects are given importance. The authors also envisage that the economic, mass applicability and photophysical aspects of the individual nanoparticles would be useful in the decision making and practical utilization of the NFs as cooling fluids in photovoltaic/thermal systems.

#### Data availability

Data will be made available on request.

#### CRediT authorship contribution statement

**Velu Nandakumar:** Conceptualization, Investigation, Software, Writing – original draft. **Chandravadhana Arumugam:** Data curation, Formal analysis, Methodology, Visualization. **Padmanaban Radhakrishnan:** Data curation, Formal analysis, Methodology, Visualization. **Vellaisamy A.L. Roy:** Data curation, Formal analysis, Visualization. **Gopalan Anantha-Iyengar:** Conceptualization, Funding acquisition, Investigation, Validation, Writing – original draft, Conceptualization, Funding acquisition, Validation, Writing – original draft. **Dong-Eun Lee:** Data curation, Formal analysis, Methodology, Visualization. **Venkatramanan Kannan:** Investigation, Methodology, Supervision, Validation, Writing – original draft.

#### Declaration of competing interest

The authors declare that they have no known competing financial interests or personal relationships that could have appeared to influence the work reported in this paper.

#### Acknowledgements

The authors thank Sri Chandrasekharendra Saraswathi Viswa Mahavidyalaya, Enathur, Kanchipuram, for providing facilities to carry out this research work. This work was supported by the National Research Foundation of Korea (NRF) grant funded by the Korea government (MSIT) (No. NRF-2018R1A5A1025137 and NRF-2022R1A2C1092289).

#### Appendix A. Supplementary data

Supplementary data to this article can be found online at <https://doi.org/10.1016/j.heliyon.2024.e26163>.

#### References

- [1] S.U.S. Choi, *Enhancing thermal conductivity of fluids with nanoparticles*, in: D.A. Siginer, Wang (Eds.), *Developments and Applications of Non-newtonian Flows*, *ume 66*, ASME, New York, 1995, pp. 99–105.
- [2] Y. Alihosseini, M.Z. Targhi, M.M. Heyhat, N. Ghorbani, Effect of a micro heat sink geometric design on thermo-hydraulic performance: a review, *Appl. Therm. Eng.* 170 (2020) 114974, <https://doi.org/10.1016/j.applthermaleng.2020.114974>.
- [3] R. Barai, D. Kumar, A. Wankhade, A. Heat transfer performance of nanofluids in heat exchanger: a review, *J. Therm. Eng.* 9 (2021) 86–106, <https://doi.org/10.18186/thermal.1243398>.
- [4] D. D Kumar, A.V. Arasu, A comprehensive review of preparation, characterization, properties and stability of hybrid nanofluids, *Renew. Sustain. Energy Rev.* 81 (2018) 1669–1689, <https://doi.org/10.1016/j.rser.2017.05.257>.
- [5] N. Acharya, Spectral simulation on the flow patterns and thermal control of radiative nanofluid spraying on an inclined revolving disk considering the effect of nanoparticle diameter and solid–liquid interfacial layer, *J. Heat Tran.* 144 (2022) 092801, <https://doi.org/10.1115/1.4054595>.
- [6] N. Acharya, F. Mabood, I.A. Badruddin, Thermal performance of unsteady mixed convective Ag/MgO nanohybrid flow near the stagnation point domain of a spinning sphere, *Int. Commun. Heat Mass Tran.* 134 (2022) 106019, <https://doi.org/10.1016/j.icheatmasstransfer.2022.106019>.
- [7] G. Humnic, A. Humnic, Hybrid nanofluids for heat transfer applications—a state-of-the-art review, *Int. J. Heat Mass Tran.* 125 (2018) 82–103, <https://doi.org/10.1016/j.ijheatmasstransfer.2018.04.059>.
- [8] S. Angayarkanni, J. Philip, Review on thermal properties of nanofluids: Recent developments, *Adv. Colloid Interface Sci.* 225 (2015) 146–176, <https://doi.org/10.1016/j.cis.2015.08.014>.
- [9] S. Dinarvand, M.N. Rostami, I. Pop, A novel hybridity model for TiO<sub>2</sub>-CuO/water hybrid nanofluid flow over a static/moving wedge or corner, *Sci. Rep.* 9 (2019) 16290, <https://doi.org/10.1038/s41598-019-52720-6>.
- [10] G. Humnic, A. Humnic, Application of nanofluids in heat exchangers: a review, *Renew. Sustain. Energy Rev.* 16 (2012) 5625–5638, <https://doi.org/10.1016/j.rser.2012.05.023>.

- [11] M. Batmunkh, M.R. Tanshen, M.J. Nine, M. Myekhlai, H. Choi, H. Chung, H. Jeong, Thermal conductivity of TiO<sub>2</sub> nanoparticles based aqueous nanofluids with an addition of a modified silver particle, *Ind. Eng. Chem. Res.* 53 (2014) 8445–8451, <https://doi.org/10.1021/ie403712f>.
- [12] M.F. Nabil, W.H. Azmi, K.A. Hamid, R. Mamat, F.Y. Hagos, An experimental study on the thermal conductivity and dynamic viscosity of TiO<sub>2</sub>-SiO<sub>2</sub> nanofluids in water: ethylene glycol mixture, *Int. Commun. Heat Mass Tran.* 86 (2017) 181–189, <https://doi.org/10.1016/j.icheatmasstransfer.2017.05.024>.
- [13] K.A. Hamid, W.H. Azmi, M.F. Nabil, R. Mamat, K.V. Sharma, Experimental investigation of thermal conductivity and dynamic viscosity on nanoparticle mixture ratios of TiO<sub>2</sub>-SiO<sub>2</sub> nanofluids, *Int. J. Heat Mass Tran.* 116 (2018) 1143–1152, <https://doi.org/10.1016/j.ijheatmasstransfer.2017.09.087>.
- [14] K.A. Hamid, W.H. Azmi, M.F. Nabil, R. Mamat, Experimental investigation of nanoparticle mixture ratios on TiO<sub>2</sub>-SiO<sub>2</sub> nanofluids heat transfer performance under turbulent flow, *Int. J. Heat Mass Tran.* 118 (2018) 617–627, <https://doi.org/10.1016/j.ijheatmasstransfer.2017.11.036>.
- [15] G.M. Moldoveanu, A.A. Minea, G. Huminic, A. Huminic, Al<sub>2</sub>O<sub>3</sub>/TiO<sub>2</sub> hybrid nanofluids thermal conductivity: an experimental approach, *J. Therm. Anal. Calorim.* 137 (2019) 583–592, <https://doi.org/10.1007/s10973-018-7974-4>.
- [16] D. Madhesh, S. Kalaiselvam, Energy efficient hybrid nanofluids for tubular cooling applications, *Appl. Mech. Mater.* 592 (2014) 922–926, <https://doi.org/10.4028/www.scientific.net/AMM.592-594.922>.
- [17] E.V. Timofeeva, J.L. Routbort, D. Singh, Particle shape effects on thermophysical properties of alumina nanofluids, *J. Appl. Phys.* 106 (2009) 014304, <https://doi.org/10.1063/1.3155999>.
- [18] Y. Jiang, X. Zhou, Y. Wang, Effects of nanoparticle shapes on heat and mass transfer of nanofluid thermocapillary convection around a gas bubble, *Microgravity Sci. Technol.* 32 (2020) 67–77, <https://doi.org/10.1007/s12217-019-09757-z>.
- [19] P. Kanti, K.V. Sharma, R.S. Khedkar, T.U. Rehman, Synthesis, characterization, stability, and thermal properties of graphene oxide based hybrid nanofluids for thermal applications: experimental approach, *Diam. Relat. Mater.* 128 (2022) 109265, <https://doi.org/10.1016/j.diamond.2022.109265>.
- [20] R. Anand, A. Raina, M. Irfan Ul Haq, M.J. Mir, O. Gulzar, M.F. Wani, M.F. Synergism of TiO<sub>2</sub> and graphene as nano-additives in bio-based cutting fluid—an experimental investigation, *Tribol. Trans.* 64 (2021) 350–366, <https://doi.org/10.1080/10402004.2020.1842953>.
- [21] S. Wang, Y. Li, H. Zhang, Y. Lin, Z. Li, W. Wang, Q. Wu, Y. Qian, H. Hong, C. Zhi, Enhancement of thermal conductivity in water-based nanofluids employing TiO<sub>2</sub>/reduced graphene oxide composites, *J. Mater. Sci.* 51 (2016) 10104–10115, <https://doi.org/10.1007/s10853-016-0239-3>.
- [22] H.I. Abdu, K. Eid, A.M. Abdullah, M.H. Sliem, A. Elzathary, X. Lu, Dry ice-mediated rational synthesis of edge-carboxylated crumpled graphene nanosheets for selective and prompt hydrolysis of cellulose and eucalyptus lignocellulose under ambient reaction conditions, *Green Chem.* 22 (16) (2020) 5437–5446, <https://doi.org/10.1039/D0GC01561J>.
- [23] K. Eid, M.H. Sliem, M. Al-Ejji, A.M. Abdullah, M. Harfouche, R.S. Varma, Hierarchical porous carbon nitride-crumpled nanosheet-embedded copper single atoms: an efficient catalyst for carbon monoxide oxidation, *ACS Appl. Mater. Interfaces* 14 (36) (2022 Aug 29) 40749–40760, <https://doi.org/10.1021/acsami.2c06782>.
- [24] Q. Lu, A. Abdelgawad, J. Li, K. Eid, Non-Metal-Doped porous carbon nitride nanostructures for photocatalytic green hydrogen production, *Int. J. Mol. Sci.* 23 (2022 Dec 1) 15129, <https://doi.org/10.3390/ijms232315129>.
- [25] B. Salah, A. Abdelgawad, Q. Lu, A.K. Ipadeola, R. Luque, K. Eid, Synergistically interactive MnFeM (M= Cu, Ti, and Co) sites doped porous gC 3 N 4 fiber-like nanostructures for an enhanced green hydrogen production, *Green Chem.* 25 (15) (2023) 6032–6040, <https://doi.org/10.1039/D3GC01071F>.
- [26] K. Eid, A. Gamal, A.M. Abdullah, Graphitic carbon nitride-based nanostructures as emergent catalysts for carbon monoxide (CO) oxidation, *Green Chem.* 25 (4) (2023) 1276–1310, <https://doi.org/10.1039/D2GC02748H>.
- [27] X. Zou, Y. Yang, H. Chen, X.L. Shi, S. Song, Z.G. Chen, Hierarchical meso/macro-porous TiO<sub>2</sub>/graphitic carbon nitride nanofibers with enhanced hydrogen evolution, *Mater. Des.* 202 (2021 Apr 1) 109542, <https://doi.org/10.1016/j.matdes.2021.109542>.
- [28] K. Atacan, M. Özacar, Construction of a non-enzymatic electrochemical sensor based on CuO/g-C<sub>3</sub>N<sub>4</sub> composite for selective detection of hydrogen peroxide, *Mater. Chem. Phys.* 266 (2021) 124527, <https://doi.org/10.1016/j.matchemphys.2021.124527>.
- [29] H. Liu, Y. Zhang, Y.P. Dong, X.F. Chu, Synthesis of ZnO/g-C<sub>3</sub>N<sub>4</sub> nanocomposite and its electrochemical application in hydrogen peroxide detection, *Russ. J. Electrochem.* 57 (2021) 808–815, <https://doi.org/10.1134/S1023193520120125>.
- [30] M.A. Mingyan, Yuling Zhai, X.U.A.N. Zihao, Shuguang Zhou, L.I. Zhixiang, Stability and thermal performance of ternary hybrid nanofluids, *Chem. Ind. Eng. Prog.* 40 (2021) 4179–4186, <https://doi.org/10.16085/j.issn.1000-6613.2020-1858>.
- [31] J. Mohammed Zayan, A.K. Rasheed, A. John, M. Khalid, A.F. Ismail, A. Aabid, M. Baig, Investigation on rheological properties of water-based novel ternary hybrid nanofluids using experimental and Taguchi method, *Mater* 15 (2022) 28, <https://doi.org/10.3390/ma15010028>.
- [32] H. Sadaf, S.I. Abdelsalam, Adverse effects of a hybrid nanofluid in a wavy non-uniform annulus with convective boundary conditions, *RSC Adv.* 10 (2020) 15035–15043.
- [33] M. Arif, P. Kumam, W. Kumam, Z. Mostafa, Heat transfer analysis of radiator using different shaped nanoparticles with water-based ternary hybrid nanofluid with applications: a fractional model, *Case Stud. Therm. Eng.* 31 (2022) 101837, <https://doi.org/10.1016/j.csite.2022.101837>.
- [34] H. Adun, D. Kavaz, M. Dagbasi, Review of ternary hybrid nanofluid: synthesis, stability, thermophysical properties, heat transfer applications, and environmental effects, *J. Clean. Prod.* 328 (2021) 129525, <https://doi.org/10.1016/j.jclepro.2021.129525>.
- [35] R.R. Sahoo, V. Kumar, Development of a new correlation to determine the viscosity of ternary hybrid nanofluid, *Int. Commun. Heat Mass Tran.* 111 (2020) 104451, <https://doi.org/10.1016/j.icheatmasstransfer.2019.104451>.
- [36] Z. Xuan, Y. Zhai, M. Ma, Y. Li, H. Wang, Thermo-economic performance and sensitivity analysis of ternary hybrid nanofluids, *J. Mol. Liq.* 323 (2021) 114889, <https://doi.org/10.1016/j.icheatmasstransfer.2019.104451>.
- [37] N.A. Muzaidi, M.A. Fikri, K.N. Wong, A.Z. Sofi, R. Mamat, N.M. Adenam, M.Y. Yunin, H.K. Adli, Heat absorption properties of CuO/TiO<sub>2</sub>/SiO<sub>2</sub> trihybrid nanofluids and its potential future direction towards solar thermal applications, *Arab. J. Chem.* 14 (4) (2021) 103059, <https://doi.org/10.1016/j.arabjch.2021.103059>, 103059, 14.
- [38] R.R. Sahoo, Thermo-hydraulic characteristics of radiator with various shape nanoparticle-based ternary hybrid nanofluid, *Powd. Technol.* 370 (2020) 19–28, <https://doi.org/10.1016/j.powtec.2020.05.013>.
- [39] Z.C. Yang, X. Li, J. Wang, Intrinsically fluorescent nitrogen-containing carbon nanoparticles synthesized by a hydrothermal process, *Carbon* 49 (2011) 5207–5212, <https://doi.org/10.1016/j.carbon.2011.07.038>.
- [40] M.H. Esfe, S. Saedodin, O. Mahian, S. Wongwises, Thermophysical properties, heat transfer and pressure drop of CO-OH-functionalized multi walled carbon nanotubes/water nanofluids, *Int. Commun. Heat Mass Tran.* 58 (2014) 176–183, <https://doi.org/10.1016/j.icheatmasstransfer.2014.08.037>.
- [41] A.H. Abdelrazek, O.A. Alawi, S.N. Kazi, N. Yusoff, Z. Chowdhury, A.A.D. Sarhan, New approach to evaluate the impact of thermophysical properties of nanofluids on heat transfer and pressure drop, *Int. Commun. Heat Mass Tran.* 95 (2018) 161–170, <https://doi.org/10.1016/j.icheatmasstransfer.2018.05.002>.
- [42] H. Yarmand, S. Gharehkhani, S.F. Seyed Shirazi, A. Amiri, M.S. Alehashem, M. Dahari, S.N. Kazi, Experimental investigation of thermo-physical properties, convective heat transfer and pressure drop of functionalized graphene nanoplatelets aqueous nanofluid in a square heated pipe, *Eng. Conv. Manag.* 114 (2016) 38–49, <https://doi.org/10.1016/j.enconman.2016.02.008>.
- [43] R. Mansourian, S.M. Mousavi, M. Mohammadpoor, S. Sabbaghi, Evaluation of heat transfer augmentation and pressure drop by water/ethylene glycol nanofluid, *Int. J. Refrig.* 131 (2021) 459–472, <https://doi.org/10.1016/j.ijrefrig.2021.07.023>.
- [44] M. Jarahnejad, E.B. Haghghi, M. Saleemi, N. Nikkam, R. Khodabandeh, B. Palm, M.S. Toprak, M. Muhammed, Experimental investigation on viscosity of water-based Al<sub>2</sub>O<sub>3</sub> and TiO<sub>2</sub> nanofluids, *Rheol. Acta* 54 (2015) 411–422, <https://doi.org/10.1007/s00397-015-0838-y>.
- [45] P.C. Mishra, S. Mukherjee, S.K. Nayak, A. Panda, A brief review on viscosity of nanofluids, *Int. Nano Lett.* 4 (2014) 109–120, <https://doi.org/10.1007/s40089-014-0126-3>.
- [46] R. Prasher, D. Song, J. Wang, P. Phelan, Measurements of nanofluid viscosity and its implications for thermal applications, *Appl. Phys. Lett.* 89 (2006) 133108, <https://doi.org/10.1063/1.2356113>.
- [47] S. Samaneh Sadeghi, A. Hadi, M.M. Mashhadi, Viscosity of Fe<sub>2</sub>O<sub>3</sub>-Water nanofluids by molecular dynamics simulations: effects of nanoparticle content, temperature and size, *J. Mol. Liq.* 382 (2023) 121859, <https://doi.org/10.1016/j.molliq.2023.121859>.

- [48] M. Rashmi, R. Padmanaban, V. Karthikeyan, V.A.L. Roy, A.I. Gopalan, G. Saianand, W.J. Kim, K. Venkatramanan, A comparative evaluation of physicochemical properties and photocatalytic efficiencies of cerium oxide and copper oxide nanofluids, *Catal* 10 (2020) 34, <https://doi.org/10.3390/catal10010034>.
- [49] I.M. Mahbulul, R. Saidur, M.A. Amalina, Latest developments on the viscosity of nanofluids, *Int. J. Heat Mass Tran.* 55 (2012) 874–885, <https://doi.org/10.1016/j.ijheatmasstransfer.2011.10.021>.
- [50] S. Ravichandran, Acoustic and thermodynamic properties of cholesterol in ethanol and 1-propanol solution in different concentration at 303K, *Res. J. Chem. Sci.* 1 (2015) 12–17.
- [51] S.S. Murshed, P. Estellé, A state of the art review on viscosity of nanofluids, *Renew. Sustain. Energy Rev.* 76 (2017) 1134–1152, <https://doi.org/10.1016/j.rser.2017.03.113>.
- [52] W. Ahmed, S.N. Kazi, Z.Z. Chowdhury, M.R. Johan, S. Mehmood, M.E. Soudagar, M.A. Mujtaba, M. Gul, M.S. Ahmad, Heat transfer growth of sonochemically synthesized novel mixed metal oxide ZnO+Al<sub>2</sub>O<sub>3</sub>+TiO<sub>2</sub>/DW based ternary hybrid nanofluids in a square flow conduit, *Renew. Sustain. Energy Rev.* 145 (2021) 111025, <https://doi.org/10.1016/j.rser.2021.111025>.
- [53] S.M. Mousavi, F. Esmaeilzadeh, X.P. Wang, Effects of temperature and particles volume concentration on the thermophysical properties and the rheological behavior of CuO/MgO/TiO<sub>2</sub> aqueous ternary hybrid nanofluid: experimental investigation, *J. Therm. Anal. Calorim.* 137 (2019) 879–901, <https://doi.org/10.1007/s10973-019-08006-0>.
- [54] A. Dezfulizadeh, A. Aghaei, A.H. Joshaghani, M.M. Najafzadeh, An experimental study on dynamic viscosity and thermal conductivity of water-Cu-SiO<sub>2</sub>-MWCNT ternary hybrid nanofluid and the development of practical correlations, *Powder Technol.* 389 (2021) 215–234, <https://doi.org/10.1016/j.powtec.2021.05.029>.
- [55] D. Yadav, A. Niral, R. Kumar, P.K. Singh, Density variation in nanofluids as a function of concentration and temperature, *Mater. Today: Proc.* 46 (2021) 6576–6580, <https://doi.org/10.1016/j.matpr.2021.04.052>.
- [56] B.C. Pak, Y.I. Cho, Hydrodynamic and heat transfer study of dispersed fluids with submicron metallic oxide particle, *Exp. Heat Tran.* 11 (1998) 151–170, <https://doi.org/10.1080/08916159808946559>.
- [57] M.M. Heyhat, A. Rajabpour, M. Abbasi, S. Arabha, Importance of nanolayer formation in nanofluid properties: equilibrium molecular dynamic simulations for Ag-water nanofluid, *J. Mol. Liq.* 264 (2018) 699–705.
- [58] J. Kurimský, M. Rajňák, M. Šárpatky, Z. Čonka, K. Paulovičová, Electrical and acoustic investigation of partial discharges in two types of nanofluids, *J. Mol. Liq.* 341 (2021) 117444, <https://doi.org/10.1016/j.molliq.2021.117444>.
- [59] M. Saraswat, R.J. Sengwa, Investigation on ethylene glycol and glycerol mixture concentration dependent optical, dielectric, electrical, rheological, and thermophysical properties of EG+Gly/ZnO semiconductor nanofluids, *Physica E Low Dimens. Syst. Nanostruct.* 150 (2023) 115700, <https://doi.org/10.1016/j.physe.2023.115700>.
- [60] K. Anu, J. Hemalatha, Ultrasonic and magnetic investigations of the molecular interactions in zinc doped magnetite nanofluids, *J. Mol. Liq.* 256 (2018) 213–223, <https://doi.org/10.1016/j.molliq.2018.02.037>.
- [61] M. Leena, S. Srinivasan, Synthesis and ultrasonic investigations of titanium oxide nanofluids, *J. Mol. Liq.* 206 (2015) 103–109, <https://doi.org/10.1016/j.molliq.2015.02.001>.
- [62] A. Nanda, A. Tiadi, S.K. Mallik, R. Giri, G. Nath, Ultrasonic characterization of silver, *Nano Fluid. IOP Conf. Ser.: Mater. Sci. Eng.* 360 (2018) 012064, <https://doi.org/10.1088/1757-899X/360/1/012064>.
- [63] R.R. Yadav, G. Mishra, P.K. Yadawa, S.K. Kor, A.K. Gupta, B. Raj, T. Jayakumar, Ultrasonic properties of nanoparticles-liquid suspensions, *Ultrason* 48 (2008) 591–593, <https://doi.org/10.1016/j.ultras.2008.06.008>.
- [64] S.A. Khan, T. Hayat, A. Alsaedi, Thermal conductivity performance for ternary hybrid nanomaterial subject to entropy generation, *Eng. Reports.* 8 (2022) 9997–10005, <https://doi.org/10.1016/j.egy.2022.07.149>.
- [65] I.L. Animasaun, Q.M. Al-Mdallal, U. Khan, A.S. Alshomrani, Unsteady water-based ternary hybrid nanofluids on wedges by bioconvection and wall stretching velocity: thermal analysis and scrutinization of small and larger magnitudes of the thermal conductivity of nanoparticles, *Mathematics* 10 (2022) 4309, <https://doi.org/10.3390/math10224309>.
- [66] I. Zahan, R. Nasrin, S. Khatun, Thermal performance of ternary-hybrid nanofluids through a convergent-divergent nozzle using distilled water-ethylene glycol mixtures, *Int. Commun. Heat Mass Tran.* 137 (2022) 106254, <https://doi.org/10.1016/j.icheatmasstransfer.2022.106254>.
- [67] E. Van der Pol, F.A.W. Coumans, A. Sturk, R. Nieuwland, T.G. Van Leeuwen, Refractive index determination of nanoparticles in suspension using nanoparticle tracking analysis, *Nano Lett.* 14 (2014) 6195–6201, <https://doi.org/10.1021/nl503371p>.
- [68] S.A. Angayarkanni, J. Philip, Effect of nanoparticles aggregation on thermal and electrical conductivities of nanofluids, *J.Nanofluids* 3 (2014) 17–25, <https://doi.org/10.1166/jon.2014.1083>.
- [69] J. Traciak, J. Sobczak, R. Kuziola, J. Wasag, G. Żyła, Surface and optical properties of ethylene glycol-based nanofluids containing silicon dioxide nanoparticles: an experimental study, *J. Therm. Anal. Calorim.* 147 (2022) 7665–7673, <https://doi.org/10.1007/s10973-021-11067-9>.
- [70] Wei Yu, Huaqing Xie, Lifei Chen, Li Yang, Investigation of thermal conductivity and viscosity of ethylene glycol based ZnO nanofluid, *Therm. Chim. Acta* 491 (2009) 92–96, <https://doi.org/10.1016/j.tca.2009.03.007>.
- [71] S.M.S. Murshed, K.C. Leong, C. Yang, Enhanced thermal conductivity of TiO<sub>2</sub>—water based nanofluids, *Int. J. Therm. Sci.* 44 (2005) 367–373, <https://doi.org/10.1016/j.ijthermalsci.2004.12.005>.
- [72] M. Sahooli, S. Sabbaghi, M. Shariaty Niassar, Preparation of CuO/Water Nanofluids Using Polyvinylpyrrolidone and a survey on its stability and thermal conductivity, *Int. J. Nanosci. Nanotechnol.* 8 (2012) 27–34.
- [73] V.S. Sai Kumar, K.V. Rao, Investigation of ultrasonic parameters of ZnO - ethylene glycol nanofluids, *J. Ovonic Res.* 13 (2017) 91–99.
- [74] K. Parekh, Thermo-magnetic properties of ternary polydispersed Mn<sub>0.5</sub>Zn<sub>0.5</sub>Fe<sub>2</sub>O<sub>4</sub> ferrite magnetic fluid, *Solid State Commun.* 187 (2014) 33–37, <https://doi.org/10.1016/j.ssc.2014.02.005>.
- [75] A. Boroomandpour, D. Toghraie, M. Hashemian, A comprehensive experimental investigation of thermal conductivity of a ternary hybrid nanofluid containing MWCNTs-titania-zinc oxide/water-ethylene glycol (80:20) as well as binary and mono nanofluids, *Synth. Met.* 268 (2020) 116501, <https://doi.org/10.1016/j.synthmet.2020.116501>.
- [76] C. Duraivathi, J. Jeya Priya, J. Poongodi, H. Johnson Jeyakumar, Ultrasonic study of molecular interactions in organic liquid with CCl<sub>4</sub> at different temperature, *Mater. Today Off.: SAVE Proc.* 49 (2022) 1968–1972, <https://doi.org/10.1016/j.matpr.2021.08.140>.
- [77] K. Venkatramanan, R. Padmanaban, V. Arumugam, Acoustic, thermal and molecular interactions of Polyethylene Glycol (20003000, 6000), *Phys. Procedia* 70 (2015) 1052–1056, <https://doi.org/10.1016/j.phpro.2015.08.224>.
- [78] S. Priyanka, O.P. Chimankar, Intermolecular interaction in the binary mixture of B-alanine with water at 323K, *Int. J. Sci. Res. Phys. Appl. Sci.* 1 (2013) 10–11.
- [79] M.K. Rawat, Sangeeta, Ultrasonic study of molecular interactions and compressibility behavior of strontium soaps in chloroform propylene glycol mixture, *Indian J. Pure Appl. Phys.* 46 (2008) 187–192.
- [80] S. Al-Ansari, S. Wang, A. Barifcani, M. Lebedev, S. Iglauer, Effect of temperature and SiO<sub>2</sub> nanoparticle size on wettability alteration of oil-wet calcite, *Fuel* 206 (2017) 34–42, <https://doi.org/10.1016/j.fuel.2017.05.077>.
- [81] R. Mondragon, J.E. Julia, A. Barba, J.C. Jarque, Characterization of silica-water nanofluids dispersed with an ultrasound probe: a study of their physical properties and stability, *Powder Technol.* 224 (2012) 138–146, <https://doi.org/10.1016/j.powtec.2012.02.043>.
- [82] L. Vandsburger, Synthesis and covalent surface modification of carbon nanotubes for preparation of stabilized nanofluid suspensions, Master of Engineering thesis, McGill University, Canada (2009). <https://escholarship.mcgill.ca/concern/theses/q811km27k>.
- [83] A.I. Ramadhan, W.H. Azmi, R. Mamat, K.A. Hamid, S. Norsakinah, Investigation on stability of tri-hybrid nanofluids in water-ethylene glycol mixture, *IOP Conf. Ser. Mater. Sci. Eng.* 469 (2019) 012068, <https://doi.org/10.1088/1757-899X/469/1/012068>.